RESONANT GLUING BIFURCATIONS

ROBERT W. GHRIST
School of Mathematics
Center for Dynamical Systems and Nonlinear Studies
Georgia Institute of Technology
Atlanta GA 30332-0160 USA

September 27, 1999

Abstract

We consider the codimension-three phenomenon of homoclinic bifurcations of flows containing a pair of orbits homoclinic to a saddle point whose principal eigenvalues are in resonance. We concentrate upon the simplest possible configuration, the so-called "figure-of-eight," and reduce the dynamics near the homoclinic connections to those on a two-dimensional locally invariant centre manifold. The ensuing *resonant gluing bifurcations* exhibit features of both gluing bifurcations and resonant homoclinic bifurcations. Under certain twist conditions, the bifurcation structure is extremely rich, although describing zero-entropy flows. The analysis carefully exploits the topology of the orbits, the centre manifold, and the parameter space.

1 Introduction

Homoclinic connections are crucial mechanisms for global changes in the dynamics of flows. It follows from the definition (an orbit that is forwards and backwards asymptotic to a single fixed point) that such a connection iteratively reinjects nearby portions of the phase space into the region near the fixed point, where stretching or contraction may take place. There are now numerous examples of homoclinic bifurcations which lead to very complicated dynamics and which appear to be ubiquitous in physical models.

The philosophy of this paper is to carefully record and exploit the topology of the system considered. Such topological information can be derived both from the embedding of homoclinic connections within invariant manifolds, as well as from the arrangement of the curves of homoclinic connections within the appropriate parameter space.

The critical vector fields whose bifurcations we consider are a produced by superimposing two well-known degeneracies: an eigenvalue resonance and a multiple connection. In §2, we recall the bifurcations associated to these individual degeneracies. In §3.1 we will briefly cite the tools introduced independently by Homburg, Sanstede, and Rousseau and Roussarie to reduce the dynamics to an invariant two-manifold. We then present a collection of topological and dynamical lemmas used to establish the bifurcation features of §4.

This analysis was motivated by a problem in the behaviour of three weakly-coupled oscillators [BGKM91]. In this work, the authors consider the bifurcation of homoclinic connections on 2-tori with the possibility of eigenvalue resonances. This paper solves and extends Problem 25 of [BGKM91]. A related result for the ori-

entable case in a near-Hamiltonian context has been proved recently by Han et al. [HC98]. The symmetric versions of these bifurcations in the orientable and nonorientable case were presented by Homburg [Hom93].

2 Resonant and gluing bifurcations

The bifurcations we consider are a simple combination of two well-known homoclinic bifurcations, a complete understanding of which is vital to the remainder of this work; hence, we review the unfoldings.

2.1 Resonant homoclinic bifurcations

We first recall the well-known phenomenon of *resonant homoclinic bifurcation*, first identified and analyzed by Leontovich in 1951 (under much more restrictive conditions than are now commonly assumed) and later considered by several including Chow et al. [CDF90] and Kokubu [Kok87, Kok88]. Let X be a vector field on $\mathbb{R}^n$ satisfying the following:

R1 X is C^K for some $K \geq 7$.

R2 X has two *principal eigenvalues* at p. That is, among the eigenvalues of DX_p, there exist real eigenvalues $\lambda^s < 0 < \lambda^u$ of multiplicity one such that $\Re e(\lambda) \notin [\lambda^s, \lambda^u]$ for all other eigenvalues λ.

R3 The linearization at p satisfies a *resonance condition*; specifically, the principal eigenvalues are in 1:1 resonance, or

$$-\lambda^s = \lambda^u. \tag{1}$$

R4 X contains an orbit Γ homoclinic to the fixed point p.

There are certain other non-degeneracy requirements concerning a careful examination of the inclination and general position of the stable and unstable manifolds associated with Γ. As these are generically satisfied, we do not further obfuscate these introductory remarks. Of the above specifications, (R3) and (R4) are structurally unstable: each contributes one codimension to the bifurcation. Item (R3) above is the crucial *local* degeneracy for obtaining interesting behavior, while item (R4) is the *global* degeneracy which makes this a global bifurcation. In addition, the *twist* of the homoclinic orbit Γ, that is the twisting associated to the local stable or unstable manifold to Γ, must be well-defined. The parity of this twist strongly influences the bifurcation.

Consider a continuous two-parameter family of vector fields, $\mathcal{X}_{l,m}$, for which $\mathcal{X}_{0,0}$ satisfies the appropriate conditions above. It is shown in Chow, Deng, and Fiedler [CDF90]; Kokubu [Kok88]; and in Kisaka, Kokubu, and Oka [KKO93], that there is a local (C^{K-2}) change of parameters from (l, m) to (Λ, μ) such that:

- $\Lambda = \frac{\lambda^s}{\lambda^u} - 1$ controls the principal eigenvalue ratio. Away from zero, the fixed point p is no longer in resonance.
- μ controls the separation of $W^s(p)$ and $W^u(p)$. Specifically, at $\mu = 0$, $W^s(p)$ and $W^u(p)$ intersect along Γ. For $\mu \neq 0$ sufficiently small, the stable and unstable manifolds of p are disjoint and the homoclinic connection is destroyed.

The ensuing bifurcation diagram depends on the parity of the twist of the homoclinic connection. For an orientable local stable manifold, the diagram is given as Figure 1. The unfolding in the non-orientable case is presented in Figure 2. In both cases, the Λ-axis is a curve of homoclinic connections. In the orientable case, a curve of saddle-node bifurcations of a periodic orbit appears for $\Lambda > 0$, below which a pair of periodic

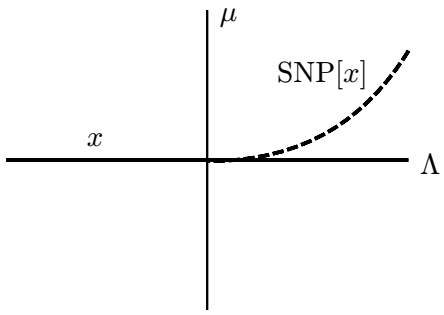

Figure 1: The unfolding of an orientable resonant bifurcation.

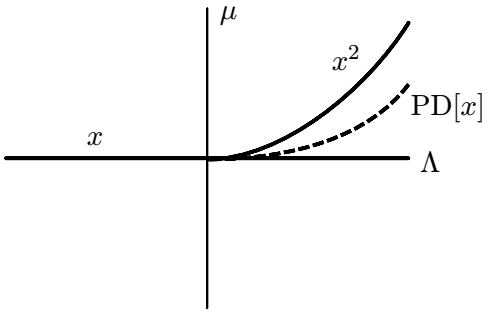

Figure 2: The unfolding of a non-orientable resonant bifurcation. Here, x^2 refers to a curve of twice-rounding homoclinic orbits.

orbits appears. In the non-orientable case, a similar curve of period-doubling bifurcations of periodic orbits appears for $\Lambda > 0$, above which the periodic orbit sheds a "twice-rounding" orbit of opposite stability type. This new orbit dies when the parameters reach the ensuing curve of twice-rounding homoclinic connections.

The moral of this review is that the presence of an eigenvalue resonance has drastically different behaviour (saddle-node; period doubling plus twice-rounding homoclinic) depending on the orientation type of the connection (orientable; non-orientable).

2.2 Gluing bifurcations

We now recall a very different sort of homoclinic bifurcation: the *gluing bifurcation* of Gambaudo et al. [GGT88]. Whereas the resonant homoclinic bifurcation is a codimension two phenomenon resulting from a single homoclinic orbit in the presence of an eigenvalue degeneracy, the gluing bifurcation results from a *double* homoclinic connection: again, a codimension two scenario. Specifically, the gluing bifurcation occurs for vector fields X on $\mathbb{R}^n$ satisfying the following:

G1 X is C^{1+}; that is, C^1 with uniformly Lipschitz partials.

G2 At the hyperbolic fixed point p, DX_p has principal eigenvalues $\lambda^s < 0 < \lambda^u < |\lambda^s|$. All other eigenvalues have real part less than λ^s.

G3 There are no first order resonances among the eigenvalues; that is,

$$\Re e(\lambda_i) \neq \lambda^u + \Re e(\lambda_j) \qquad \forall\, i, j. \quad (2)$$

G4 X has two homoclinic connections at the fixed point p which are bounded away from any other fixed point. Denote these connections Γ_x, Γ_y.

As before, there are additional conditions concerning the twist of the homoclinic orbits — these are generically satisfied.

Note that conditions (G2) and (G3) imply that the principal eigenvalues are not in resonance and that in particular the unstable principal eigenvalue is dominated by the stable eigenvalues. Intuitively, one thinks of the flow in a neighborhood of the fixed point as being contracted in all directions but one (that corresponding to λ^u). Along that sole unstable direction, the expansion is weaker than the contraction occuring elsewhere. This *local* feature, when coupled with the *global* double homoclinic connection permits interesting behavior.

We will, as before, examine a neighborhood W of $\Upsilon = \Gamma_x \cup \Gamma_y \cup \{p\}$ for C^1 perturbations of X. Such perturbations preserve properties (G1) through (G3) above. Since Υ is bounded away from other fixed points and W is a small tubular neighborhood of Υ, orbits in W cannot "double back" and must follow Υ monotonically. In fact, the eigenvalue assumption (G2) implies that there is an attractor contained in W consisting of closed orbits and/or homoclinic connections. One describes such orbits symbolically by labeling Γ_x, Γ_y with the letters x, y and then assigning to any periodic orbit γ in W a finite acyclic word in x and y given by what order γ travels around each loop: this is the orbit's *itinerary*. More precisely, we have a shift equivalence class of words, since beginning at a different point yields a cyclic permutation of the word. One can likewise define an itinerary for a homoclinic connection; however, since these orbits have a definite beginning and end, there is an induced ordering on the itinerary. Thus, periodic orbits are described by shift-equivalence classes of words and homoclinic connections by ordered words.

Certain vector fields near X support periodic or homoclinic orbits with nontrivial itineraries, e.g., x^2yxy. Which itineraries are possible is at the heart of understanding the gluing bifurcation. It is a fact stated in [GGT84, GGT85] and proved in [GGT88] that any periodic orbit in W in the unfolding of X must have a *rotation compatible* itinerary. That is, it may be obtained as the symbol sequence of a point $z \in I$ under iteration by a rotation map $\rho_\theta : z \mapsto (z + \theta) mod\ 1$ with the partition $I_x = (0, 1-\theta]$, $I_y = (1-\theta, 1]$ for some $\theta \in [0, 1)$. Given such a word, the unique θ for that word is called the *rotation number*. Note: to compute the rotation number from a given rotation compatible word, divide the number of y's by the total length of the word: e.g., $x^2yxy \Rightarrow \theta = \frac{2}{5}$. Alternatively, one can describe rotation compatible words as those whose letters are "evenly distributed," or built from the blocks $x^k y, x^{k+1}y$ (or xy^k, xy^{k+1}) for some k.

The main result concerning gluing bifurcations is the following [GGT88]:

Theorem 2.1 *There is a neighborhood W of Υ which contains at most two periodic orbits for every sufficiently small C^1 perturbation of a critical system. Any periodic orbits which may be present are attracting and have rotation compatible itineraries. If there are two periodic orbits, then their associated rotation numbers are Farey neighbors.*

We recall that two rational numbers $\frac{p}{q}$ and $\frac{p'}{q'}$ are *Farey neighbors* if $\mid pq' - qp' \mid = 1$.

The fact that at most two periodic orbits exist follows from the observation that the attractor lies within the closure of the one dimensional unstable manifold $W^u(p)$, of which there are two "sides" (separated by p). Although Theorem 2.1 severely restricts the number and type of periodic orbits near Υ, there is nevertheless enough latitude within many such systems to allow for bifurcation diagrams with infinitely many curves [GGT84], as we shall see.

As with the resonant homoclinic bifurcation, we examine a two-parameter family of vector fields. In this case, one is able to choose unfolding parameters μ and ν which independently control the breaking of each homoclinic connection Γ_x, Γ_y (resp.). Each parameter is then analogous to the parameter μ in the unfolding of the resonant homoclinic bifurcation.

Again, as in the unfolding of the resonant homoclinic bifurcation, the twist along the homoclinic connections are crucial. There are three different possibilities:

1. **orientable**: both connections have orientable local stable manifolds.
2. **semi-orientable**: one connection is orientable, the other is not.
3. **non-orientable**: neither connection is orientable.

The bifurcation diagrams for the three above cases in the figure-of-eight configuration are given as Figures 3 through 5. A complete catalogue of unfoldings for the gluing bifurcation in various configurations can be found scattered throughout the literature.

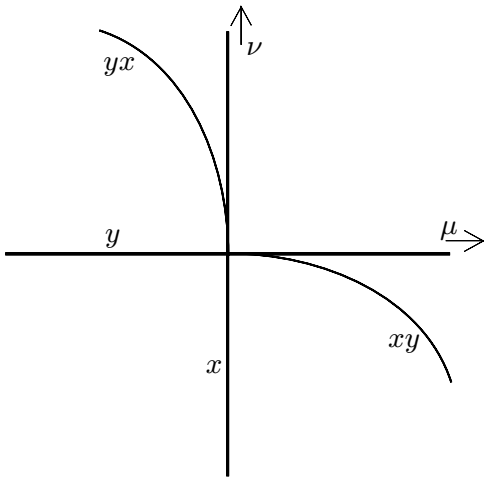

Figure 3: The unfolding of an orientable gluing bifurcation.

This bifurcation derives its name from the following corollary: in every configuration, along the diagonal in parameter space $\mu = \nu < 0$ there are two periodic orbits, x and y, whose periods grow as the parameters approach zero, at which point the double homoclinic connection exists. Then, for $\mu = \nu > 0$, the double homoclinic connection breaks so as to form a *single* "glued" periodic orbit of itinerary xy.

3 Resonant gluing bifurcations

In this section, we consider the codimension three scenario of combining a gluing bifurcation with an eigenvalue resonance. Surprisingly complex bifurcation sequences can result, especially in the presence of twisted homoclinic connections. We focus on the simplest possible case: namely, when the two homoclinic curves are in the so-called figure-of-eight configuration (*cf.*

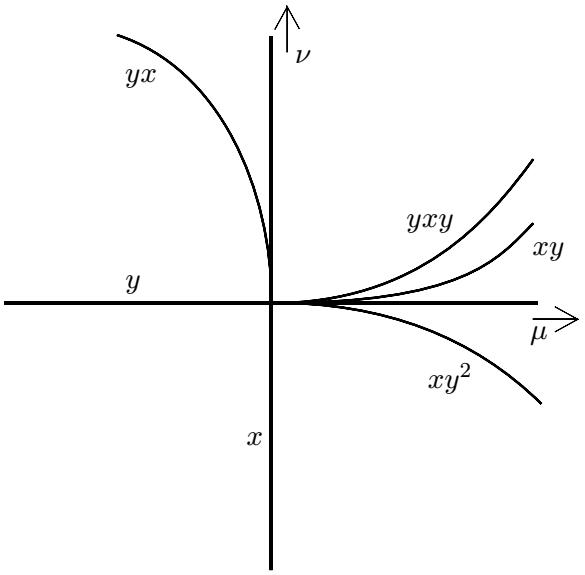

Figure 4: The unfolding of a semi-orientable gluing bifurcation.

the gluing bifurcation analysis of §2.2), and the local dynamics are such that a reduction to a two-dimensional centre manifold is possible.

In the case where the homoclinics are in an alternate configuration, say, a butterfly or a spiral, the associated bifurcations are significantly more complex since the passage through a resonance creates horseshoes in the dynamics. See the remarks in §5.

3.1 Reduction of the dynamics

Earlier in the 1990s, several authors proved theorems which allow one to reduce dynamics near homoclinic connections to low-dimensional centre manifolds. The idea is as follows: given a homoclinic connection Γ (including the fixed point p), consider $W^{cs}_{loc}(\Gamma) \cap W^{cu}_{loc}(\Gamma)$, the intersection of the local weak-stable and weak-unstable manifolds. One then proves that the relevant dynamics can be captured by the restriction to this (or some nearby invariant) manifold.

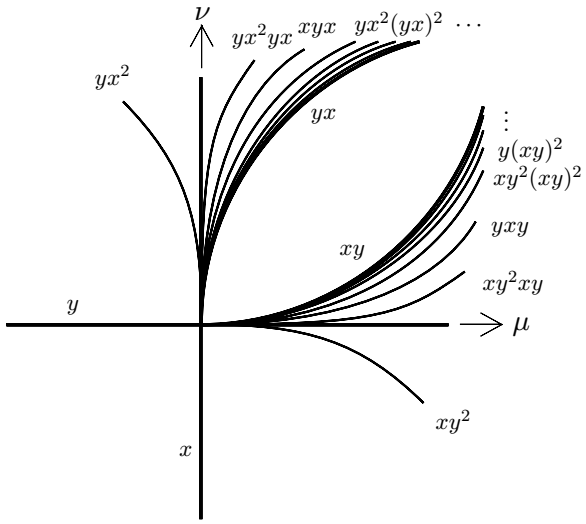

Figure 5: The unfolding of an orientable gluing bifurcation. There is a sequence of homoclinic curves accumulating onto the yx curve in the order $\{(yx)^k y^2 x, (yx)^k y\}_{k=0}^{\infty}$ (and likewise interchanging x and y).

In the early 1990s, Homburg [Hom93], relying heavily on the work of [HPS70], proceeded to do just this for the case of single and double homoclinic connections. Sanstede [San93] proved an analogous theorem almost simultaneously. In the more recent work of Rousseau and Roussarie [RR96], the authors use surprisingly effective techniques from the theory of planar flows to accomplish a similar task. Their work explicitly considers the problem of a pair of resonant homoclinic connections; however, their results hold true only for a flow which is originally of dimension three.

By stringing together the elements in this body of work, it is possible to obtain the following very strong result.

Theorem 3.1 *Under the conditions R1, R2, R3, and G4 above, the dynamics in a neighborhood of the homoclinic connections possesses an invariant two-dimensional centre manifold $\mathcal{T}$ which captures all the local invariant sets.*

From now on we assume that we are working on a two-dimensional local invariant centre manifold $\mathcal{T}$ in a neighborhood of a pair of homoclinic connections in the figure-of-eight configuration. In order to understand the dynamics, we consider a pair of local transversals e_1 and e_2 to the local stable manifolds of the equilibrium (the top and bottom of Figure 6). Place coordinates on these intervals having zero at $e_i \cap W^s(p)$ and with the positive direction pointing to the right (as presented in Figure 6).

Proposition 3.2 *The cross-sectional return maps on e_1 and e_2 are given as:*

$$\begin{array}{lll} \phi_{11} : e_1^+ \to e_1 & ; & z \mapsto a_x z^{\Lambda+1} - \mu \\ \phi_{21} : e_2^+ \to e_1 & ; & z \mapsto -a_x z^{\Lambda+1} - \mu \\ \phi_{22} : e_2^- \to e_2 & ; & z \mapsto -a_y (-z)^{\Lambda+1} + \nu \\ \phi_{12} : e_1^- \to e_2 & ; & z \mapsto a_y (-z)^{\Lambda+1} + \nu \end{array} \tag{3}$$

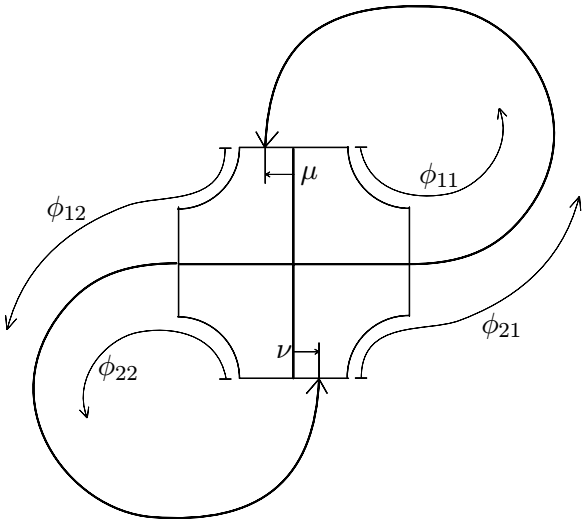

Figure 6: The portion of the local centre manifold $\mathcal{T}$ near the equilibrium, with return maps on transversals.

For details, see the thesis of Homburg [Hom93]. Without a loss of generality we may assume that the coefficients a_x and a_y are greater than one in absolute value (otherwise, switch the sign of Λ). The sign of a_x and a_y determines the twist of the

homoclinic orbits Γ_x and Γ_y respectively: negative coefficients imply nonorientable twisting.

3.2 Topology of admissible orbits

The fact that all the relevant dynamics occurs on an invariant manifold of dimension two implies that there are serious constraints on the types of periodic orbits and homoclinic connections which may be present.

As in the case of the gluing bifurcation of §2.2, we label the two principal non-contractible loops in $\mathcal{T}$ as x and y. This allows us to assign to each periodic orbit on $\mathcal{T}$ an itinerary, or word in $\{x, y\}$, which is well-defined up to shift equivalence. Given a word $\mathbf{w}$, we will denote its shift-equivalence class by $[\mathbf{w}]$; *e.g.*, $[x^2yxy] = [yxyx^2]$. In the case of a homoclinic connection, there is a unique ordered itinerary since homoclinic connections have both beginning and end. Given a word $\mathbf{w}$, we will denote by $\mathbf{w}^{-1}$ the "inverse" word given by writing $\mathbf{w}$ backwards.

The following propositions explore the constraints on admissible itineraries given the global topology of $\mathcal{T}$:

Proposition 3.3 *Any itinerary* $\mathbf{w}$ *which appears as a periodic orbit or homoclinic connection on* $\mathcal{T}$ *must satisfy* $[\mathbf{w}] = [\mathbf{w}^{-1}]$*; that is, the itinerary is shift-equivalent to itself written backwards.*

Proof: Consider the case where one has a homoclinic connection on $\mathcal{T}$. We may perturb the system slightly to transform this connection into a periodic orbit with the same itinerary. Hence, assume that $[\mathbf{w}]$ represents the periodic orbit γ on $\mathcal{T}$. Since the itinerary is defined in terms of the fundamental group $\pi_1(\mathcal{T})$, it is invariant with respect to isotoping the orbit γ or the manifold $\mathcal{T}$.

Note that $\mathcal{T}$ may be isotoped so as to have a symmetry about the diagonal line as sketched in Figure 7. We claim that γ may be isotoped to be invariant under this symmetry. Since the symmetry map *reverses* the orientation on γ induced by the flow direction, the itinerary $\mathbf{w}$ would necessarily be the same (up to shifts) when read backwards, *i.e.*, $\mathbf{w}^{-1}$.

We now show that γ can be made invariant under the symmetry. Consider the submanifold $\tilde{\mathcal{T}} \subset \mathcal{T}$ given by cutting off the arms of $\mathcal{T}$, as in Figure 7. As per the diagram, label the four extremal edges of $\tilde{\mathcal{T}}$ as $e_1, \ldots, e_4$. From Figure 6, the global return maps send $e_3 \mapsto e_1$ and $e_4 \mapsto e_2$; hence, the number of points in $\gamma \cap e_1$ and $\gamma \cap e_3$ are equal (resp. $\gamma \cap e_2$ and $\gamma \cap e_4$) and can be isotoped so as to be evenly spaced on the edges.

There are four types of curves on $\tilde{\mathcal{T}}$ up to isotopy: see Figure 7. The collection of curves which goes from e_1 to e_3 can be isotoped so that each is invariant under the diagonal symmetry. The same holds for curves going from e_2 to e_4. By a counting argument, the number of curves connecting e_2 to e_3 must equal the number of curves going from e_1 to e_4. Hence, these curves may be isotoped so that, as collections of curves, they are invariant under the symmetry; hence, the curves restricted to $\tilde{\mathcal{T}}$ are invariant.

Each "arm" of $\mathcal{T}$ which was removed to form $\tilde{\mathcal{T}}$ is topologically a square $I \times I$ with side edges $e_1 \cup e_2$ or $e_3 \cup e_4$. The intersection of γ with this $I \times I$ is a set of horizontal lines, and the action of the symmetry map on this square is reflection about the vertical axis. It follows that the symmetry map respects γ on $\mathcal{T} - \tilde{\mathcal{T}}$ and hence on all of $\mathcal{T}$. $\diamond$

Note that this does rule out certain itineraries: *e.g.*, xyx^2y^2.

Proposition 3.4 *At most two homoclinic connections can coexist on* $\mathcal{T}$*; furthermore, if* $\mathbf{u}$ *and* $\mathbf{v}$ *are ordered itineraries representing coexistent homoclinic connections on* $\mathcal{T}$*, then the initial symbols of* $\mathbf{u}$ *and* $\mathbf{v}$ *differ (likewise with the final symbols).*

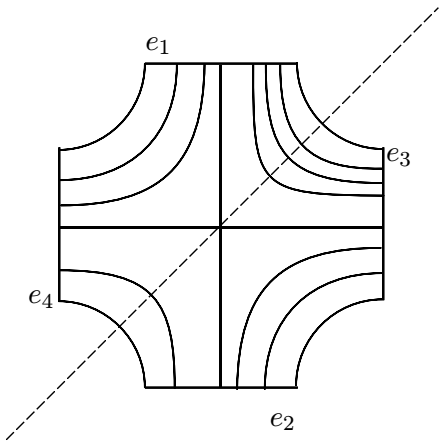

Figure 7: Reflecting about the diagonal leaves the centre manifold $\mathcal{T}$ invariant. There are four types of curves on the portion of $\mathcal{T}$ near the equilibrium.

Proof: This statement follows immediately from the uniqueness theorem for ODEs on the compact two-dimensional manifold $\mathcal{T}$. $\diamond$

Proposition 3.5 *If* $\mathbf{u}$ *and* $\mathbf{v}$ *are ordered itineraries representing coexistent homoclinic connections on* $\mathcal{T}$*, then either*

1. $\mathbf{u} = \mathbf{u}^{-1}$ *and* $\mathbf{v} = \mathbf{v}^{-1}$ *(as ordered words); or*
2. *the words are* $\mathbf{u} = (xy)^k$, $\mathbf{v} = (yx)^k$, *and* $\mathcal{T}$ *is non-orientable.*

Proof: We apply the proof of Proposition 3.3 to the pair of simultaneous connections. By isotoping $\mathcal{T}$ and reflecting about the line of symmetry as above, we find that the coexistent homoclinic curves $\mathbf{u}$ and $\mathbf{v}$ are (together) preserved with time reversed; hence, as ordered words, either $\mathbf{u}$ goes to $\mathbf{u}^{-1}$ and $\mathbf{v}$ to $\mathbf{v}^{-1}$, or $\mathbf{u}$ goes to $\mathbf{v}^{-1}$. The former corresponds to case (1) of the proposition. Assume that $\mathbf{u} = \mathbf{v}^{-1}$ and, hence, $\mathbf{v} = \mathbf{u}^{-1}$. Then, from Proposition 3.4, we know that (without loss of generality), $\mathbf{u} = x\mathbf{u}'y$ for some (perhaps empty) word $\mathbf{u}'$. Assuming that $\mathbf{u}$ contains x^2 (or y^2) as a subword, the map which reflects $\mathcal{T}$ about the diagonal cannot take $\mathbf{u}$ to $\mathbf{v}^{-1}$, since the curve in $\mathcal{T}$ corresponding to the second x in the x^2-term cannot avoid being invariant under the relection: see Figure 7. Hence, the itinerary $\mathbf{u}$ is of the form $(xy)^k$ and case (2) follows. It is clear from Figure 7 that case (2) can occur only when $\mathcal{T}$ is non-orientable. $\diamond$

These simple results, derived only from the two-dimensional nature of the centre manifold $\mathcal{T}$, will prove invaluable in concluding that certain curves of homoclinic bifurcations in parameter space must connect. Specifically, in §4.2 and §4.3, we will use the fact that on a two-dimensional parameter plane of fixed Λ, a curve of homoclinic orbits of itinerary, say, xy^2xy, may not transversally intersect any other curve of homoclinics.

4 Bifurcation diagrams

In this section, we undertake the task of unfolding the simplest resonant gluing bifurcations in the three possible orientation configurations: orientable, semi-orientable, and non-orientable. We begin with the orientable case, in which the governing equations directly give the bifurcation curves. In the semi-orientable case, we make use of the local gluing bifurcation unfolding to elucidate finer structures and connect local pictures. Finally, in the non-orientable case, we require more serious and detailed arguments to pin down the surprisingly fine bifurcation structure.

In what follows, we will use the language of itineraries for periodic orbits and homoclinic connections, as described in §3.2. We will denote by H[$\mathbf{w}$] the curve of homoclinic orbits with (ordered) itinerary $\mathbf{w}$. Likewise, SN[$\mathbf{w}$] and PD[$\mathbf{w}$] will be used to represent curves of saddle-node and period-doubling (respectively) bifurcations of orbits with itinerary [$\mathbf{w}$]. In diagrams, H[x] is usually abbreviated by x, etc.

4.1 Case I: oriented

Consider the simplest case, in which $\mathcal{T}$ is an orientable manifold. In this case, the reader can see clearly (without the help of Propositions 3.3 through 3.5) that the only admissible itineraries are $[x], [y]$, and $[xy] = [yx]$. For such low periods, we may easily solve compositions of the one-dimensional return maps of Equation (3) to obtain analytic expressions for curves of homoclinic connections in the parameter space (μ, ν, Λ). For example, to find the curve of homoclinic connections H$[xy]$, we solve the equation

$$\phi_{12} \circ \phi_{21}(0) = 0 \tag{4}$$

for ν (or μ if appropriate). We summarize the results of such derivations below:

$$\begin{array}{ll} \mathrm{H}[x] & \mu = 0 \\ \mathrm{H}[y] & \nu = 0 \\ \mathrm{H}[xy] & \nu = -a_y \mu^{\Lambda+1} \\ \mathrm{H}[yx] & \mu = -a_x \nu^{\Lambda+1} \end{array} \tag{5}$$

Furthermore, when $\Lambda > 0$, we can solve for the curves of saddle-node orbits, which are to be expected from the presence of the eigenvalue resonance. To find the curve of saddle-nodes associated to the periodic orbit of itinerary x, we solve the equation $\phi_{11}(p) = p$ for μ or ν as appropriate, where p is determined by the equation

$$\left.\frac{d}{dz}\phi_{11}(z)\right|_p = 1, \tag{6}$$

Solving for the saddle-node curves of itineraries x and y yields the following:

$$\begin{array}{ll} \mathrm{SN}[x] & \mu = -a_x^{-1/\Lambda}\Lambda(1+\Lambda)^{-1-1/\Lambda} \\ \mathrm{SN}[y] & \nu = -a_y^{-1/\Lambda}\Lambda(1+\Lambda)^{-1-1/\Lambda} \end{array} \tag{7}$$

However, this is not the complete picture. We have not accounted for the effect of the resonant homoclinic bifurcation on the curve of homoclinics corresponding to the itinerary xy (or yx). By the results of §2.1, there must be a curve of saddle node bifurcations of orbits branching from the curves H$[xy]$ and H$[yx]$ along $\Lambda = 0$ opening in the positive Λ direction. We will not be concerned with the precise location of saddle-node and period-doubling curves of bifurcations in future cases: the homoclinic curves determine the bifurcation diagram. The dual facts that saddle-nodes posit no topological obstructions (an infinite sequence of alternating saddle-nodes can in principle accumulate in a narrow band of parameter space without repercussion) and that their defining equations are highly transcendental leave little hope of obtaining rigorous placement of these curves in our unfoldings. Thus, we apply Occam's razor and draw in the simplest possible scenario for SN$[xy]$ in the cross-section of parameter space given in Figure 8. The three-dimensional unfolding is given in Figure 9.

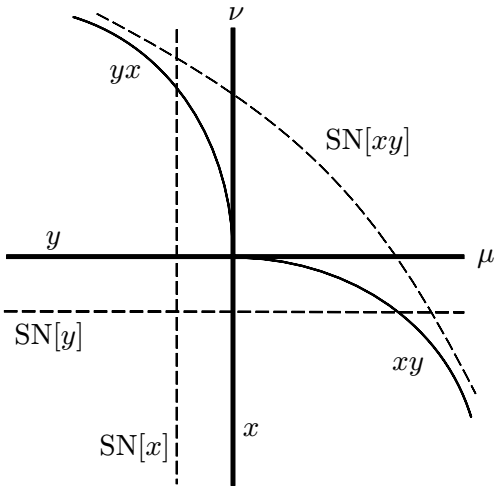

Figure 8: The unfolding of the orientable figure-of-eight resonant gluing bifurcation, $\Lambda > 0$.

We note that this picture agrees with the situation considered by Kokubu [Kok88]: given a pair of homoclinic connections passing through an eigenvalue resonance, the H$[xy]$ and H$[yx]$ curves must "flip" between being tangent to the H$[x]$ and H$[y]$ curves as Λ passes through zero. Kokubu's results are proved under very general hypotheses, but do not comment on the behaviour of higher-order curves of homoclinic orbits that we will consider in the presence of non-

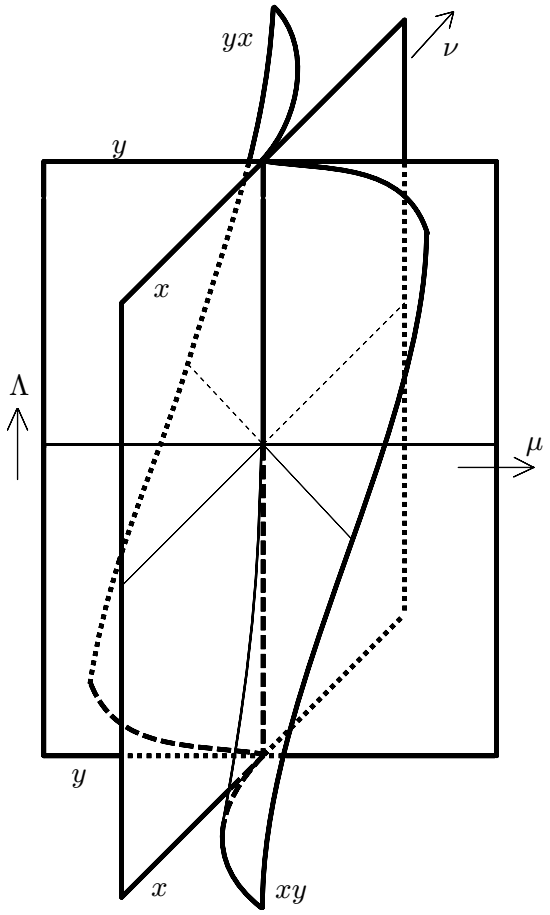

Figure 9: The unfolding of the orientable figure-of-eight resonant gluing bifurcation, homoclinic connections only.

orientable homoclinic connections.

Remark 4.1 The following observation is extremely important. Note that for fixed $\Lambda > 0$, the gluing bifurcation results may be applied to $\mathcal{T}$ to give the *local* bifurcation structure as presented in Figure 3. For $\Lambda < 0$, the theorem does not hold (since the eigenvalue ratio is of the wrong sign); however, since $\mathcal{T}$ is two-dimensional, reversing time (*i.e.*, flowing backwards) exchanges the eigenvalues λ^u and λ^s and hence changes the sign of Λ, satisfying the hypotheses for a gluing bifurcation. Upon noting that reversing time in the orientable case sends $\mu \mapsto -\mu$ and $\nu \mapsto -\nu$ and sends itineraries to their inverses, we have that the *local* picture for $\Lambda < 0$ in the orientable case is precisely as in Figure 10. Note this is in perfect agreement with the full picture of Figure 8.

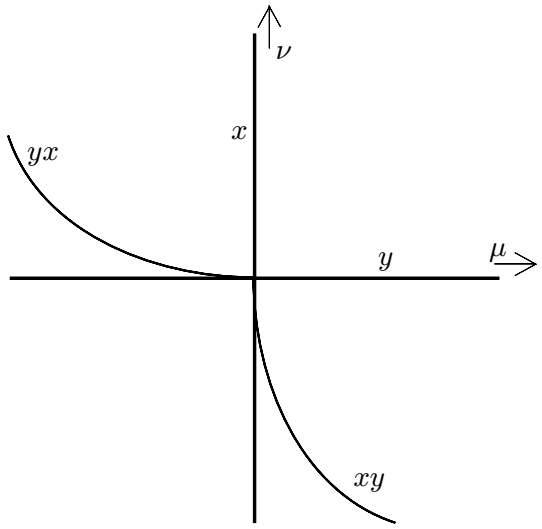

Figure 10: The local unfolding for $\Lambda < 0$ in the orientable case.

4.2 Case II: semioriented

Without a loss of generality, we may assume that the loop corresponding to x is orientable, while that of y is not orientable. By the unfolding of the standard gluing bifurcation given in §2.2, we know that for fixed $\Lambda > 0$, the bifurcation diagram appears locally as in Figure 4. As in Remark 4.1, to get the picture for $\Lambda < 0$, we may reverse time, reading the itineraries backwards and sending $\mu \mapsto -\mu$ and $\nu \mapsto \nu$. This yields the local bifurcation diagram given in Figure 11. Note that the curve of homoclinic connections $\mathrm{H}[xy^2]$ becomes for $\Lambda < 0$ the curve $\mathrm{H}[y^2x]$.

Using this as a basis for what should appear in the full bifurcation diagram, we may solve Equation (3) for certain "low-period" curves of homo-

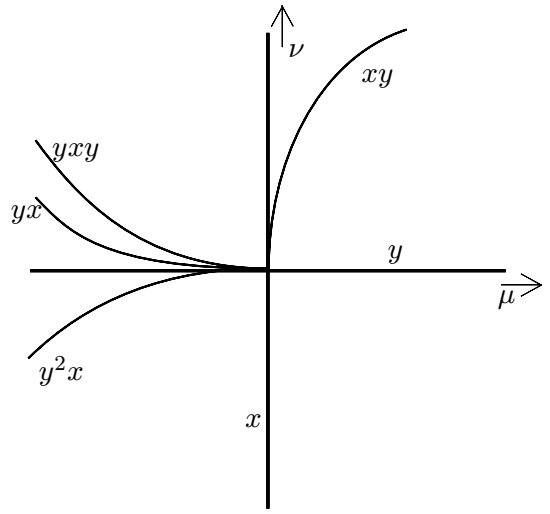

Figure 11: The local unfolding for $\Lambda < 0$ in the semi-orientable case.

clinic connections:

$$\begin{array}{ll}
\mathrm{H}[x] & \mu = 0 \\
\mathrm{H}[y] & \nu = 0 \\
\mathrm{H}[y^2] & \nu = -(-a_y)^{-1/\Lambda} \\
\mathrm{H}[xy] & \nu = -a_y \mu^{\Lambda+1} \\
\mathrm{H}[yx] & \mu = -a_x \nu^{\Lambda+1} \\
\mathrm{H}[yxy] & \mu = -a_x \nu^{\Lambda+1} + (-\nu/a_y)^{1/(\Lambda+1)} \\
\mathrm{H}[xy^2] & \mu = \left\{ \left(-\nu - (\nu/a_y)^{1/(\Lambda+1)} \right) / a_y \right\}^{1/(\Lambda+1)} \\
\mathrm{H}[y^2x] & \mu = -a_x \left(-a_y (-\nu)^{\Lambda+1} + \nu \right)^{1/(\Lambda+1)}
\end{array} \tag{8}$$

Given that the x-loop is orientable and the y-loop is not, the unfolding of the resonant bifurcation tells us that for $\Lambda > 0$ there should be a curve of saddle-node bifurcations for x and a curve of period-doubling bifurcations separating $\mathrm{H}[y]$ from $\mathrm{H}[y^2]$. We solve for the saddle-node curves as in Equation (6). To solve for the period-doubling curves about $\mathrm{H}[y]$, we likewise consider the equations $\phi_{22}(p) = p$ and

$$\left. \frac{d}{dz} \phi_{22}(z) \right|_p = -1, \tag{9}$$

and solve for ν. The analytical solutions for simple saddle-node and period-doubling curves are as follows:

$$\begin{array}{ll}
\mathrm{SN}[x] & \mu = -a_x^{-1/\Lambda} \Lambda (1+\Lambda)^{-1-1/\Lambda} \\
\mathrm{PD}[y] & \nu = -(-a_y)^{-1/\Lambda} \Lambda (1+\Lambda)^{-1-1/\Lambda} (2+\Lambda)
\end{array} \tag{10}$$

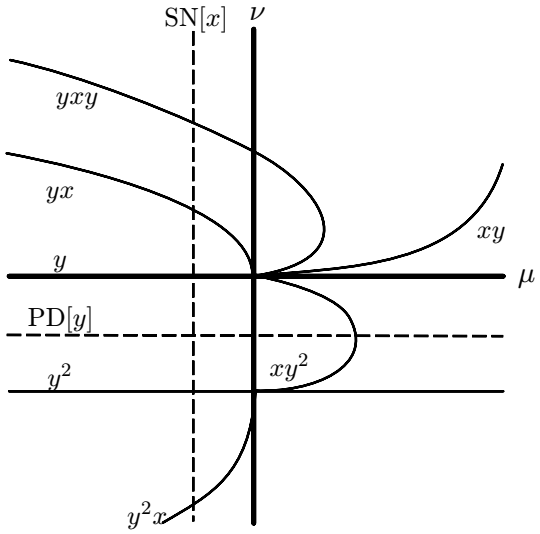

Figure 12: The partial unfolding of the semi-orientable figure-of-eight resonant gluing bifurcation: $\Lambda > 0$.

The (incomplete) bifurcation diagram appears in Figure 12. Notice that the curve $\mathrm{H}[y^2]$ transversally intersects the curve $\mathrm{H}[x]$, thus creating a new double homoclinic connection. By restricting $\mathcal{T}$ to a small tubular neighborhood of this subsidiary double homoclinic connection, a rescaling of parameter space gives us a standard gluing bifurcation. But note, we are now back to the *orientable* case, since the connection with itinerary y^2 has even parity in the twist. Hence, we know from the gluing bifurcation results that there *must* exist curves of homoclinic connections $\mathrm{H}[xy^2]$ and $\mathrm{H}[y^2x]$ which are tangent to the curves $\mathrm{H}[y^2]$ and $\mathrm{H}[x]$ respectively, as is already found in the analytical solutions of Equation (8).

However, the curves $\mathrm{H}[x]$ and $\mathrm{H}[yxy]$ also intersect transversally. As above, this yields an orientable gluing bifurcation: there must exist curves $\mathrm{H}[(xy)^2]$ and $\mathrm{H}[(yx)^2]$ which are tangent,

respectively, to H[yxy] and H[x]. An analytical closed-form solution for these curves is not possible, and, although a numerical solution would be sufficient, it is possible to completely characterise these bifurcation curves by appealing to the topology of the parameter plane and of $\mathcal{T}$ as follows. Consider the branch of homoclinics H[$(yx)^2$]: we know from the gluing bifurcation unfolding that it emanates from the transversal intersection of H[x] and H[yxy] tangent to H[x] in the $-\nu$ direction.

Lemma 4.2 *The curve of homoclinics* H[$(yx)^2$] *does not intersect any other curve of homoclinics.*

Proof: If this curve intersects any other curve of homoclinics transversally, Proposition 3.4 states that its itinerary must be of the form $x \dots y$. However, the curve H[$(yx)^2$] is bounded in the plane by the three curves H[x], H[yxy] and H[yx]. Neither of these curves has itinerary of the proper form; hence, H[$(yx)^2$] does not cross over these boundaries transversally. If H[$(yx)^2$] intersects some other curve nontransversally, then it is born in a gluing bifurcation and its itinerary $yxyx$ must be the concatenation of the itineraries of two transversally intersecting homoclinic curves at that point. As all such curves with shorter itinerary have been explicitly found, this is impossible. ◇

Thus, we have used the topology of $\mathcal{T}$ and of the parameter space to *trap* curves of bifurcations. A nearly identical proof shows that the curve H[$(xy)^2$] is likewise trapped within the inert region bounded by the three curves H[x], H[xy], and H[yxy].

Of course, we already know from our review of the resonant bifurcation that the "doubled" homoclinic curves H[$(xy)^2$] and H[$(yx)^2$] must follow along the curves H[xy] and H[yx] respectively, each pair separated by a curve of period-doubling of orbits of itinerary $[xy] = [yx]$. This curve, along with the analogous curve of saddle-nodes of itinerary $[xy^2]$ are given in the complete unfolding of Figures 13 through 14.

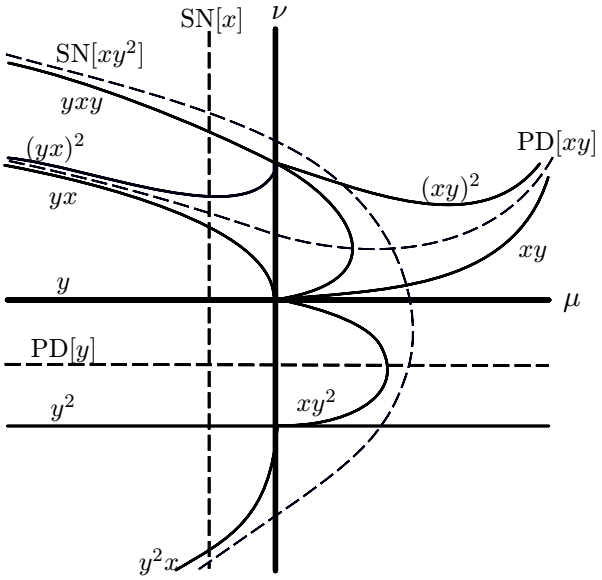

Figure 13: The full unfolding of the semi-orientable figure-of-eight resonant gluing bifurcation: $\Lambda > 0$

4.3 Case III: nonoriented

As in the previous two analyses, by reversing time we know the local form of the bifurcation diagrams at slices of constant $\Lambda > 0$ and $\Lambda < 0$. Analytical solutions give a skeletal outline of the bifurcation diagram for $\Lambda > 0$. The details of the analytical derivations are lengthy and similar to those in previous cases: the first skeletal diagram appears as Figure 15. Here, the sequence of curves accumulating on H[xy] and H[yx] can be read off from Figure 5 directly. The local picture for $\Lambda < 0$ can be obtained by interchanging x and y in Figure 5 (to account for the reversal of time).

Included in Figure 15 are several subsidiary codimension two points where two curves of homoclinics transversally intersect. As in the previous semi-orientable case, each of these will give

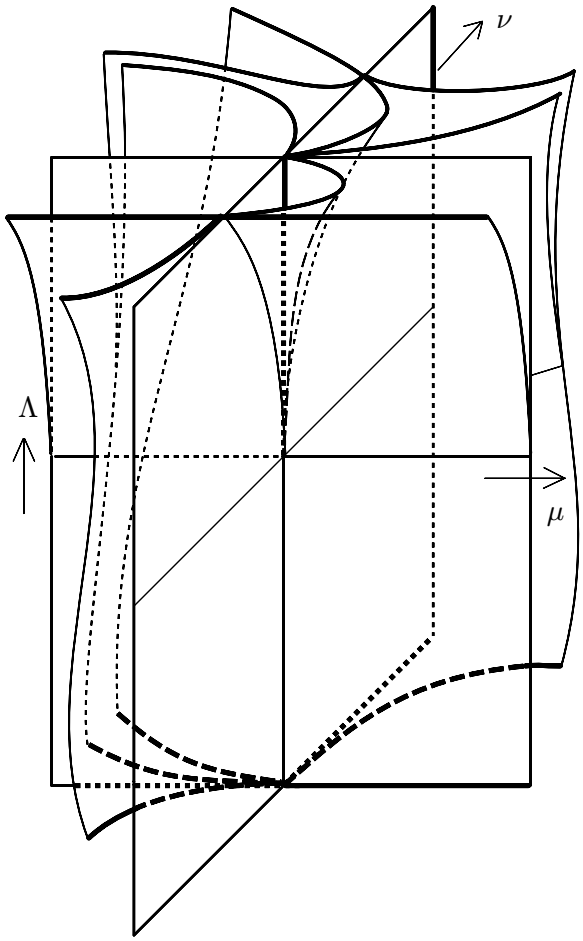

Figure 14: The full unfolding of the semi-orientable figure-of-eight resonant gluing bifurcation, homoclinic curves only.

rise to new "miniature" gluing bifurcations in a neighborhood of the intersection. Each of these is either of orientable or semi-orientable type, depending on the x- and y-parity of the itineraries so implicated. The local structure of these subsidiary curves are detailed in Figure 16.

Lemma 4.3 *The curves of homoclinic orbits which intersect the curve* $\mathrm{H}[xy^2x]$ *appear in the following order:*

$$\left\{\mathrm{H}[[y(xy)^k]^2], \mathrm{H}[y(xy)^k]\right\}_{k=0}^{\infty} \qquad (11)$$

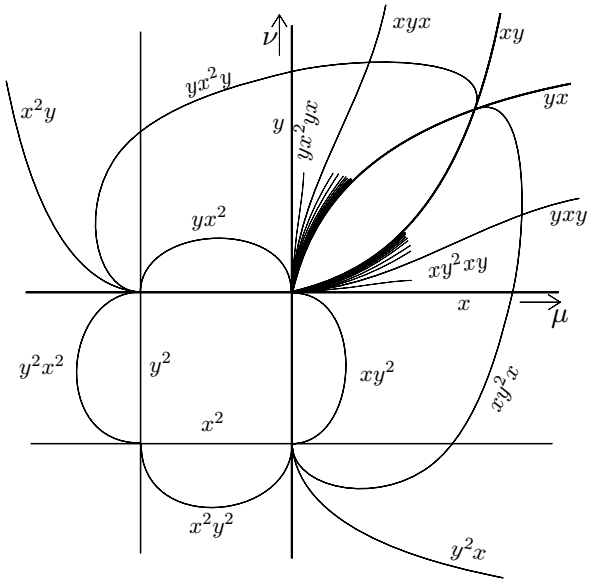

Figure 15: The skeletal bifurcation diagram derived from low-period analytical results: non-orientable case, $\Lambda > 0$.

Proof: Restrict attention to the curve $\mathrm{H}[xy^2x]$. The homoclinic orbit with itinerary xy^2x separates the centre manifold $\mathcal{T}$ into the invariant region displayed in Figure 17. The other branch of the unstable manifold of the equilibrium point must lie on this domain.

Consider the path through parameter space which traverses the $\mathrm{H}[xy^2x]$ curve from the origin to its termination point. A change of coordinates gives a 1-parameter bifurcation problem. Denote by α said parameter, normalized so that the degenerate situation $\mu = \nu = 0$ corresponds to $\alpha = 1$ and the common intersection of $\mathrm{H}[xy] \cap \mathrm{H}[yx]$ corresponds to $\alpha = 0$. The transversal illustrated in Figure 17 induces a 1-d piecewise-continuous return map P_α.

Analysis of P_α would require considering arbitrarily long sequences of iterates of the local return maps, extended somehow to account for the fact that the transversal is not a local transversal: this is extremely difficult. However, since we wish to determine only the *order* in which co-

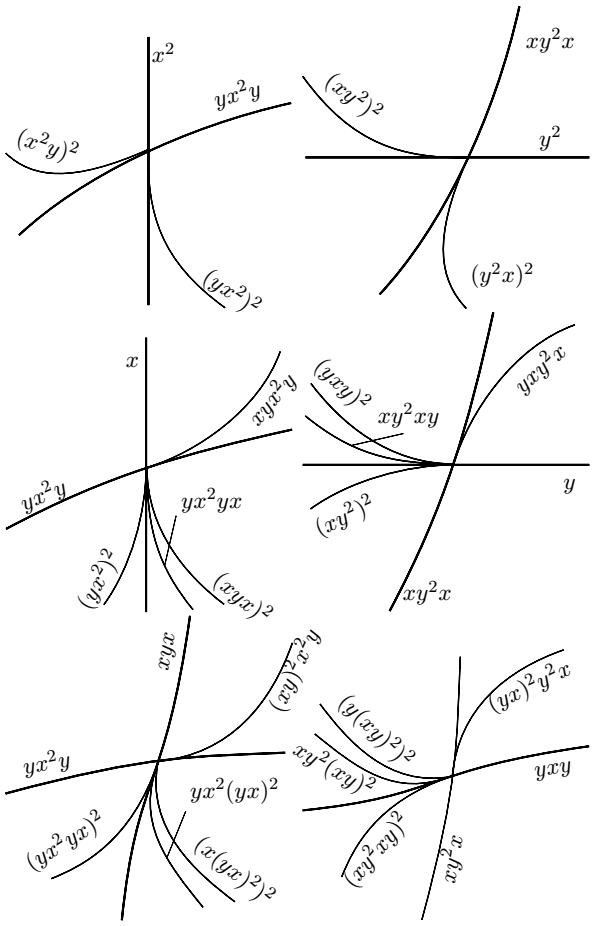

Figure 16: The partial bifurcation diagram highlighting subsidiary gluing bifurcations: non-orientable case, $\Lambda > 0$.

existent bifurcations appear, and not the precise points at which they exist, we may collapse the system to a measured foliation.[1]

[1]This construction, which appears often in the work of Thurston [Thu88], can be interpreted as taking a flow on an orientable surface and collapsing out all of the non-recurrent orbits in the flow, followed by blowing up what remains to reconstruct the surface. This yields a flow which is *transversally measured*. In this context, this means that any transverse segment is assigned a weight which is invariant under the flow — there is no essential contraction or expansion in the transverse direction to the flow. This useful construction is highly under-utilized in applied dynamical systems.

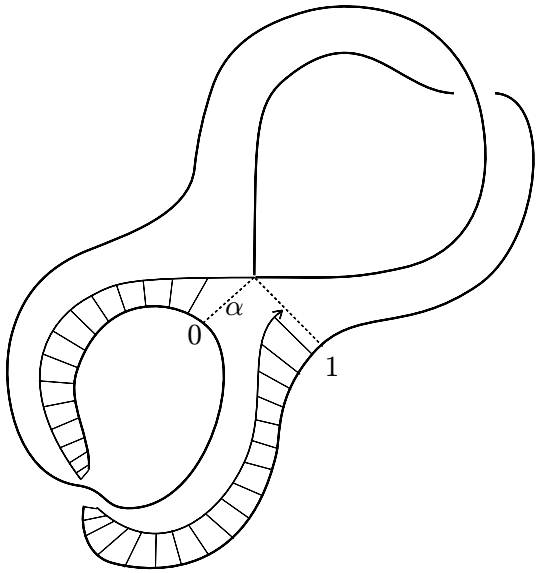

Figure 17: The invariant region carved out by the homoclinic orbit of signature xy^2x, along with a transversal (dashed lines). From this is derived a 1-d map governed by the measured foliation property: transverse curves have a flow-invariant measure.

If we assign to the first portion of the transversal of Figure 17 the weight α, the transverse-invariance uniquely defines the return map P_α:

$$P_\alpha : x \mapsto \begin{cases} 1-x & x \in (0,\alpha] \\ x-\alpha & x \in (\alpha,1) \end{cases} . \qquad (12)$$

Of course, the map is undefined at the endpoints of the interval since it is here where the curve $\mathrm{H}[xy^2x]$ degenerates. In this context, the measured foliation approximation "linearizes" the return map on the transversal without compromising the topology of the system. Every orbit of this map is periodic since it is an interval exchange map with two pieces, one of which is orientation-reversing. In particular, the itinerary of the orbit of $x = \alpha$ under P_α determines the itinerary of the second homoclinic curve which crosses $\mathrm{H}[xy^2x]$. Note from Figure 17 that the orientation reversing component of P_α corresponds to the itinerary block y while

the orientation preserving portion corresponds to the block xy.

At $\alpha = 1/(n+2)$, the corresponding orbit is:

$$\frac{1}{n+2} \longrightarrow \frac{n+1}{n+2} \longrightarrow \frac{n}{n+2} \longrightarrow \cdots \longrightarrow \frac{1}{n+2}, \tag{13}$$

hence, the itinerary for $\alpha = 1/(n+2)$ is $y(xy)^n$. Likewise, for any $\epsilon \in (0,1)$, we have

$$\frac{1}{n+2-\epsilon} \longrightarrow \frac{n+1-\epsilon}{n+2-\epsilon} \longrightarrow \cdots \longrightarrow \frac{1-\epsilon}{n+2-\epsilon} \longrightarrow \frac{n+1}{n+2-\epsilon} \longrightarrow \cdots \longrightarrow \frac{1}{n+2-\epsilon}. \tag{14}$$

Thus, the itinerary for $\alpha \in [1/(n+2), 1/(n+1))$ is $[y(xy)^n]^2$. Varying α between 1 and 0 yields the desired sequence of homoclinic crossings. $\diamond$

The places where the curves $\mathrm{H}[y(xy)^n]$ and $\mathrm{H}[[y(xy)^n]^2]$ cross $\mathrm{H}[xy^2x]$ (along with the symmetric intersections) yield an infinite sequence of subsidiary local gluing bifurcations which may interact outside of a small neighborhood of the double homoclinic points. The remainder of the bifurcation analysis is to use topological information to connect these local pictures into a global unfolding. We proceed with a series of lemmatta in the spirit of Lemma 4.2. There is a symmetry in the parameter space $\mu \leftrightarrow \nu$ which allows us to reduce the analysis in the region $\mu > \nu$: all lemmatta in the section hold true under exchanging x and y.

Lemma 4.4 *The curves* $\mathrm{H}[y(xy)^k]$ *which intersect* $\mathrm{H}[xy^2x]$ *connect to the corresponding curves emanating from the origin* $\{\mu = \nu = 0\}$.

Proof: Assume the curves do not connect. Then there must be a pair of transverse curves of homoclinics somewhere else which gives birth to a curve $\mathrm{H}[y(xy)^k]$. Hence, the word $y(xy)^k$ can be written as a combination of words $\mathbf{u}$ and $\mathbf{v}$. By Proposition 3.5, these subwords must be of the form either $\mathbf{u} = x(yx)^m$ and $\mathbf{v} = y(xy)^n$; or $\mathbf{u} = (xy)^p$ and $\mathbf{v} = (yx)^p$. The latter case cannot occur since the word $y(xy)^k$ must alternate in x and y. Thus $y(xy)^k = \mathbf{v}(\mathbf{uv})^p$, where $\mathbf{u} = x(yx)^m$ and $\mathbf{v} = y(xy)^n$. These are subwords of the same form (up to x-y symmetry); hence, $m < k$ and $n < k$. A simple induction argument on k shows that the curves connect without further interaction. $\diamond$

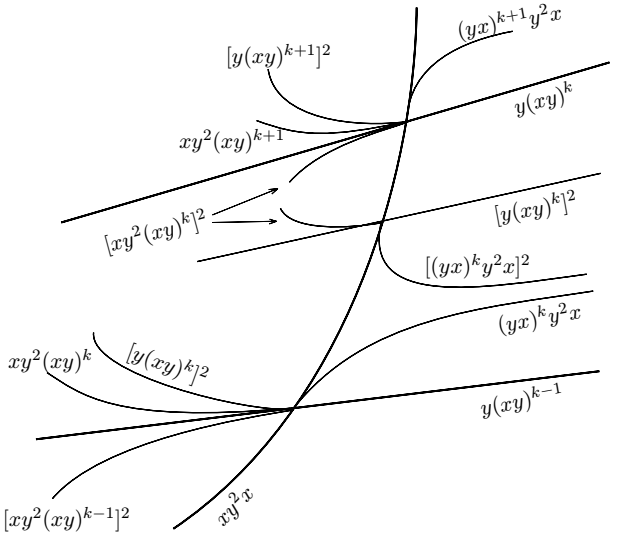

Figure 18: Local structure of high-order subsidiary gluing bifurcations along $\mathrm{H}[xy^2x]$: nonorientable case, $\Lambda > 0$.

Given the local structure about the curves transverse to $\mathrm{H}[xy^2x]$, we can deduce a wealth of subsidiary gluing bifurcations. All of the points at which the curves $\mathrm{H}[[y(xy)^k]^2]$ and $\mathrm{H}[y(xy)^k]$ cross $\mathrm{H}[xy^2x]$ are codimension-two gluing bifurcations which alternate between orientable and semi-orientable type respectively. In Figure 18, we illustrate the local bifurcation structure along a portion of the curve $\mathrm{H}[xy^2x]$ induced by the local subsidiary gluing bifurcations.

At this stage, it is apparent that the loose ends of the bifurcation diagram come in pairs which we would like to say must match up; indeed, our unfolding of the semiorientable resonant gluing bifurcation suggests precisely these connections. However, since the bifurcation results we derive hold *locally* in the full three-dimensional parameter space, we cannot conclude that the local pictures connect in the obvious manner without fur-

ther interactions. Rather, we use trapping techniques to obtain the final picture.

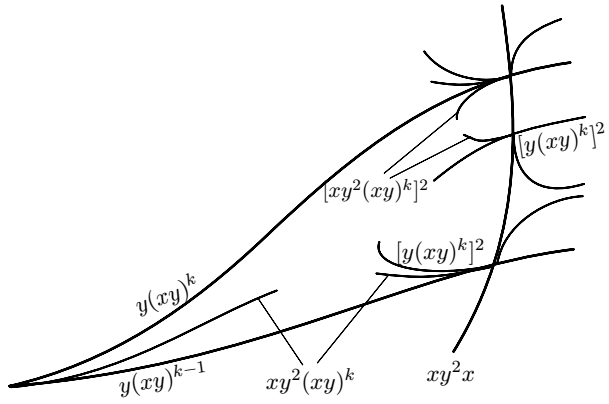

Figure 19: The trapping region for connecting pairs of homoclinic curves.

Lemma 4.5 *The homoclinic curves of itinerary* $\mathrm{H}[xy^2(xy)^k]$ *in Figure 19 connects to the corresponding curve emanating from the origin* $\mu = \nu = 0$. *In addition, the pair of curves of type* $\mathrm{H}[[xy^2(xy)^k]^2]$ *in Figure 19 connects without further interactions.*

Proof: Consider the curve $\mathrm{H}[xy^2(xy)^k]$. By Proposition 3.5, this cannot transversally intersect any other curve of homoclinics; hence, if the two known ends with this itinerary do not connect, they must each terminate at another gluing bifurcation. Assume then that $\mathrm{H}[xy^2(xy)^k]$ is born in another codimension-2 point. Again by Proposition 3.5, the two words $\mathbf{u}$ and $\mathbf{v}$ which compose $xy^2(xy)^k$ would have to be palindromes of the form $\mathbf{u} = x...x$, $\mathbf{v} = y...y$. From the form of the itinerary, it follows that either $\mathbf{u} = x$ and $\mathbf{v} = y$ or $xy^2(xy)^k = \mathbf{uv}$, where $\mathbf{u} = xy^2x$ and $\mathbf{v} = y(xy)^{k-1}$. These two intersections are the only possible termination points, which are ruled out by prior analysis.

A nearly-identical argument works for connecting the curves of doubled orbits $\mathrm{H}[[xy^2(xy)^k]^2]$. ◇

Lemma 4.6 *The pair of homoclinic curves of itinerary* $\mathrm{H}[[y(xy)^k]^2]$ *in Figures 18 and 19 connects without further interactions.*

Proof: This word is a palindrome, so Proposition 3.5 is not applicable. However, by Proposition 3.4, the curve $\mathrm{H}[[y(xy)^k]^2]$ is prohibited from exiting the region of the parameter plane bounded by the curves $\mathrm{H}[xy^2(xy)^k]$, $\mathrm{H}[y(xy)^k]$, and $\mathrm{H}[[xy^2(xy)^k]^2]$. The sole recourse is that $\mathrm{H}[[y(xy)^k]^2]$ crosses $\mathrm{H}[xy^2x]$ more than once. However, doing so would create new curves of $\mathrm{H}[[xy^2(xy)^k]^2]$, which, as shown in Lemma 4.5, must terminate in an already-occupied intersection between $\mathrm{H}[x(yx)^k]$ and $\mathrm{H}[xy^2x]$. See Figure 19 for the trapping region $\mathcal{A}$ in which our loose ends are constrained.

All given curves within $\mathcal{A}$ are non-palindromes and hence "inert" (excluded from further transverse intersections) with the exception of $\mathrm{H}[y(xy)^k]$. This curve is a palindrome, and so is susceptible to an "invasion" by a curve of homoclinics from outside the region $\mathcal{A}$. Such an intrusion could create a new codimension-2 point, perhaps spawning additional curves of the form $\mathrm{H}[[y(xy)^k]^2]$. That this cannot occur is seen in two ways. First, the curve $\mathrm{H}[y(xy)^k]$ is "guarded" by the curve $\mathrm{H}[xy^2(xy)^{k+1}]$. By Lemma 4.5, this curve connects from the origin to the intersection of $\mathrm{H}[x(yx)^k]$ with $\mathrm{H}[xy^2x]$, and by Proposition 3.5, this curve is inert. Thus, no additional interactions can occur within the trapping region $\mathcal{A}$, and the curves must connect.

For another proof, note that if a foreign curve were to intersect $\mathrm{H}[x(yx)^k]$, then the itinerary of every additional curve "born" in the intersection would be composed of combinations of $x(yx)^k$ with some other word. Any such combination, or subsidiary combinations thereof, could not compose the word $[x(yx)^k]^2$. Hence, again, the curves must connect. ◇

At this stage we are finished with the bifurcation diagram, as concerns the placement of homoclinic orbits, since all of the "loose ends" have

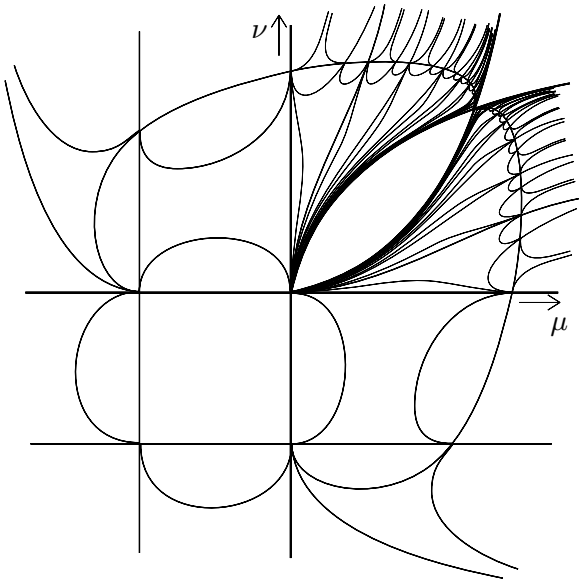

Figure 20: The full unfolding of the non-orientable figure-of-eight resonant gluing bifurcation: homoclinic connections only, $\Lambda > 0$.

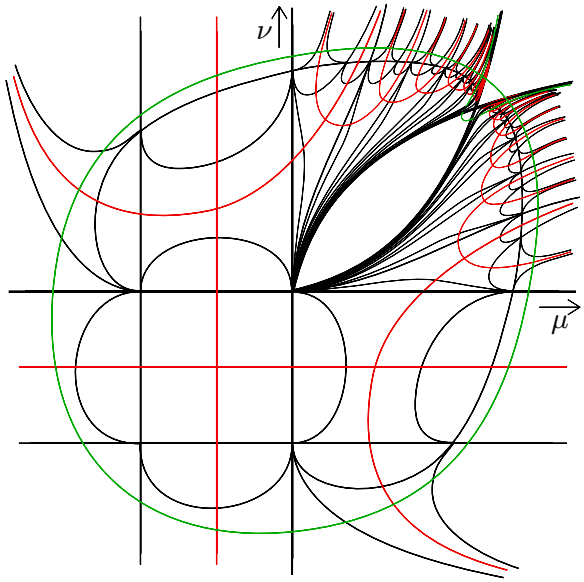

Figure 21: The full unfolding, including saddle-node and period-doubling curves: $\Lambda > 0$.

been accounted for. There are two important features which ensure that the diagram is correct. First, note that near each homoclinic orbit with odd-twist (that is, with an odd number of symbols in the itinerary), there is a subsidiary "doubled" homoclinic connection nearby. Second, consider the ordering of homoclinic connections around a circle of large radius centered a the origin. It so happens that the itineraries appear (along with their doubles) in precisely the ordering prescribed by the gluing bifurcation when $\Lambda < 0$; hence, as Λ decreases through zero, the complex region of curves in the bifurcation diagram shrinks to the origin, leaving the homoclinic curves which proceed in the order prescribed by the gluing bifurcation of Figure 5. Our finished diagram for the $\Lambda > 0$ plane appears as Figure 20. Itineraries for the curves are not listed but can be derived from Figures 15 and 18.

The existence of saddle-node and period-double bifurcation curves is not dealt with in detail here. Given the analysis of the prior two types of resonant gluing bifurcations, we know which curves will throw off which types of bifurcations for $\Lambda > 0$. For saddle-node bifurcations, there are two cases to consider. (1) The curve SN$[x^2y^2]$ surrounds the "bubble" formed by H$[x^2y^2]$, H$[y^2x^2]$, H$[xy^2x]$, and H$[yx^2y]$. (2) The intersection of the curves H$[xy]$ and H$[yx]$ gives a symmetry-breaking pitchfork bifurcation from which emanates two curves of saddle-nodes — this phenomenon has been detailed in [PTT87] and elsewhere. The remaining period-doubling curves can be roughly found by considering the local picture near each local resonant bifurcation and piecing together the curves in the natural way. In Figure 21, we detail the rough structure of these curves. Finally, in Figure 22, we give the full, three-dimensional diagram for the unfolding of this bifurcation.

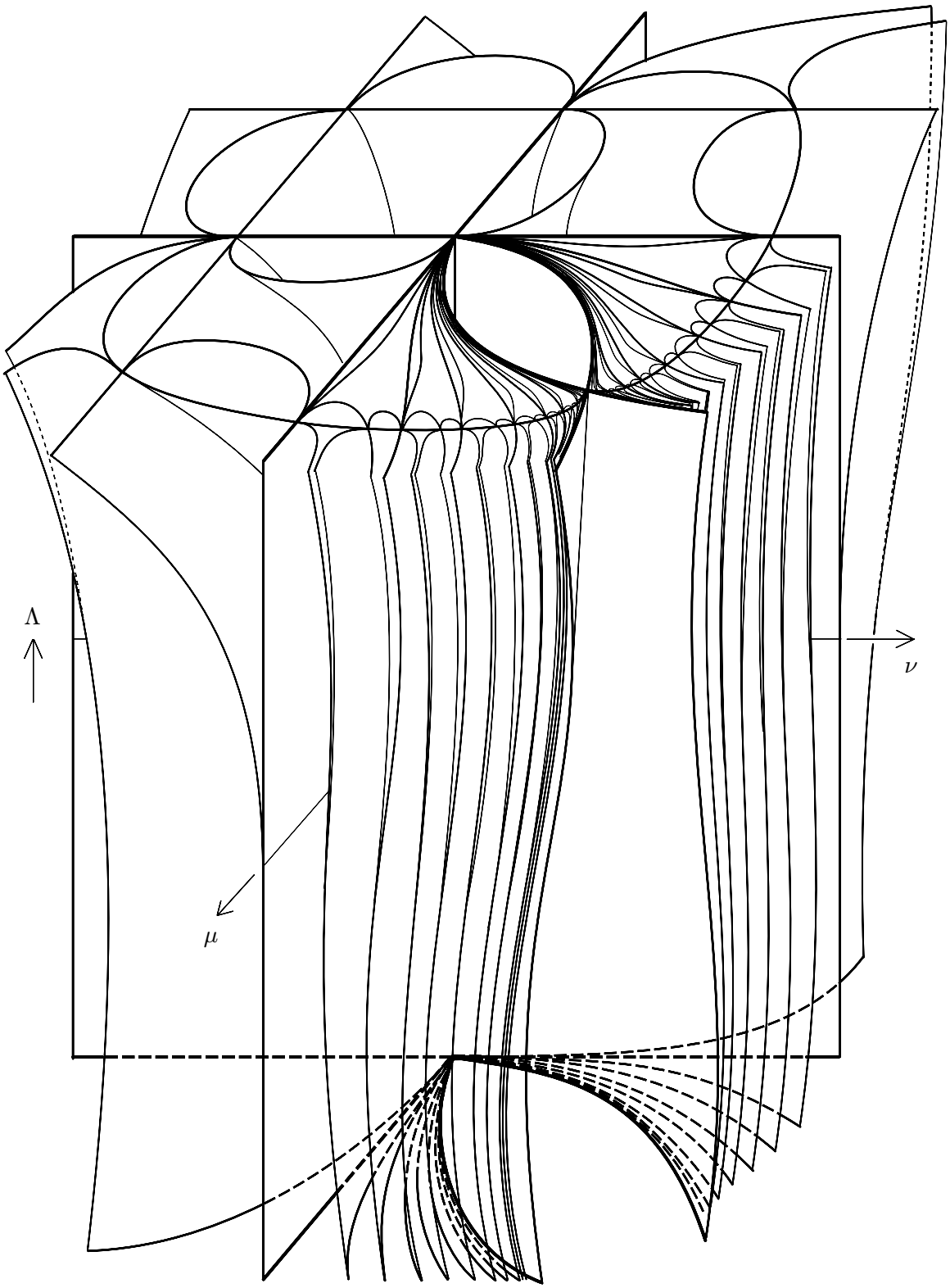

Figure 22: The full unfolding of the non-orientable figure-of-eight resonant gluing bifurcation, homoclinic curves only.

5 Other configurations

The figure-of-eight configuration unfolded in this work is but the simplest possibility for a resonant gluing bifurcation. All of the other possible configurations are inherently more complex: the reduction to a two-dimensional centre manifold is impossible and the reversibility arguments used in this work are invalid. Thus, positive entropy flows always arise on the expansive side of the bifurcation diagrams. However, this does not completely obscure the bifurcation structure.

Consider the butterfly and spiral configurations illustrated in Figure 23. The butterfly configuration (reminiscent of the Lorenz system) again has three sub-cases depending upon the twist associated to the homoclinic curves. The spiral configuration, while not having a well-defined twist, is nonetheless more complicated, as even the local picture for the non-resonant gluing bifurcation is not completely understood.

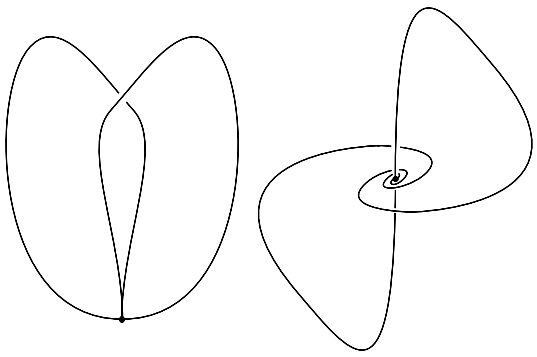

Figure 23: The butterfly (left) and spiral (right) configurations.

For the butterfly case, one can use the theory of *templates*, or branched 2-manifolds, to reduce the corresponding three-dimensional centre manifolds to a more manageable object (see [GHS97] for a complete treatment of these objects). Here, the resonance parameter changes the branched manifold from having contractive to expansive dynamics. A similar analysis to the one carried out in this work reveals the "routes" to positive entropy flows in the butterfly configuration. We do not include details given the background in template theory required, as well as the fact that many of the bifurcation diagrams become too complicated to rigorously analyze. The bifurcation diagrams in Figure 24 through Figure 26 should be thus considered as conjectural. These figures show cross-sectional slices for $\Lambda > 0$. Only the homoclinic curves are drawn: it is obvious where the associated saddle-node and period-doubling bifurcation curves must lie to make the diagrams consistent. Appropriate labelings for itineraries of homoclinic curves are not given in these figures (for clarity). Itineraries can be easily ascertained by applying local gluing bifurcation rules for the butterfly configurations (see, *e.g.*, [HG94]).

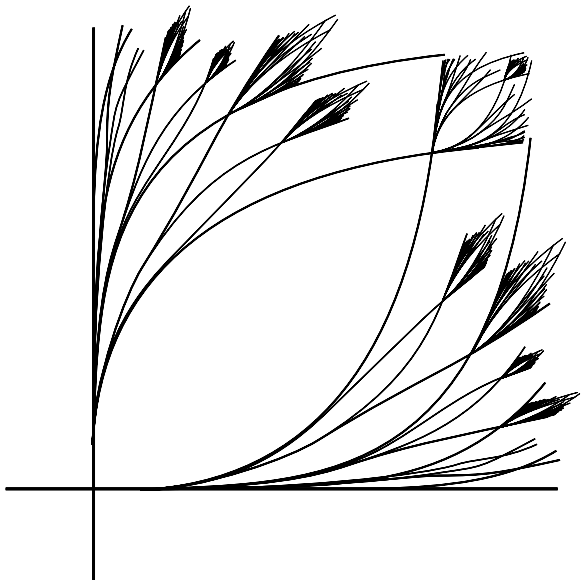

Figure 24: The unfolding of the orientable butterfly resonant gluing bifurcation, $\Lambda > 0$.

The spiral configurations are, as mentioned, much more complicated. It remains an open problem to precisely determine the fine bifurcation structures present in the non-resonant case: the resonant gluing bifurcations pose further difficulties.

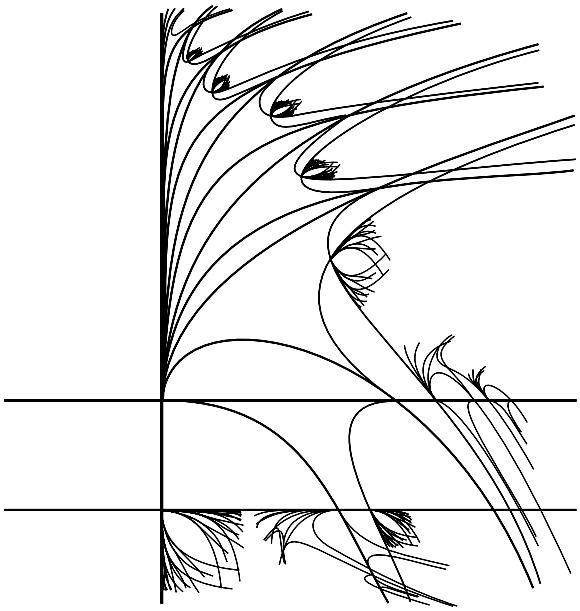

Figure 25: The unfolding of the semiorientable butterfly resonant gluing bifurcation, $\Lambda > 0$.

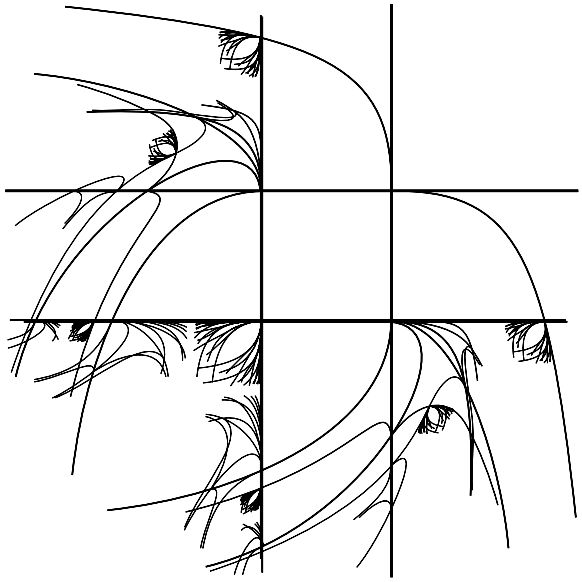

Figure 26: The unfolding of the nonorientable butterfly resonant gluing bifurcation, $\Lambda > 0$.

6 Conclusion

In this paper, we have considered the cumulative effects of simultaneous resonant and gluing bifurcations of a pair of homoclinic connections in the simplest figure-of-eight configuration. The twisting of the homoclinic orbits is especially relevant to the complexity of the bifurcation structure, which can be extremely rich in the nonorientable case.

We note that there may be extensions of this analysis to certain configurations of heteroclinic connections.

In the course of this paper, we have unfolded the resonant necklace configuration, in the language of [BGKM91]: the authors considered the case of a pair of resonant homoclinic orbits for a flow on a torus. As the torus is an orientable surface, such orbits must form a figure-eight configuration with both loops orientable. Of greater interest is the case where one or, in particular, both loops are nonorientable: such dynamics must take place in a flow of dimension three or higher. It is a remarkable feature of these systems that a family of zero-entropy flows can possess such intricate bifurcation structures which can be explicitly detailed. Any global bifurcations which involve systems acquiring positive entropy are hopelessly complex.

One principal motivation for investigating gluing bifurcations is the fact that they implicate *attracting* orbits. Hence, such bifurcations should be (and are [MP87]) observed in physical systems. One example of a model for which numerical work indicates the existence of an orientable resonant gluing bifurcation is a smooth model for an electric circuit with cubic nonlinearity studied by Khibnik et al [KRC93].

ACKNOWLEDGMENTS

The author wishes to thank the Center for Applied Mathematics at Cornell University, where this work was begun. Conversations with John Guckenheimer, Phil Holmes, Alexander Khibnik, and others were invaluable.

References

[BGKM91] C. Baesens, J. Guckenheimer, S. Kim, and R. MacKay. Three coupled oscillators: mode-locking, global bifurcations and toroidal chaos. *Physica D*, 49:387–475, 1991.

[CDF90] S. N. Chow, B. Deng, and B. Fiedler. Homoclinic bifurcation at resonant eigenvalues. *J. Dynam. Diff. Eqs.*, 2(2):177–244, 1990.

[GGT84] J.-M. Gambaudo, P. Glendinning, and C. Tresser. Collage de cycles et suites de Farey. *C. R. Acad. Sc. Paris*, 299:711–714, 1984.

[GGT85] J.-M. Gambaudo, P. Glendinning, and C. Tresser. Stable cycles with complicated structure. *J. Physique Lett.*, 46 (15):653–657, 1985.

[GGT88] J.-M. Gambaudo, P. Glendinning, and C. Tresser. The gluing bifurcation I: symbolic dynamics of the closed curves. *Nonlinearity*, 1:203–214, 1988.

[GHS97] R. Ghrist, P. Holmes, and M. Sullivan. *Knots and Links in Three-Dimensional Flows*, volume 1654 of *Springer Lecture Notes in Mathematics*. Springer-Verlag, Berlin, Heidelberg, New York, 1997.

[HC98] M. Han and J. Chen. On the number of limit cycles in double homoclinic bifurcations. Technical Report CDSNS98-308, Georgia Institute of Technology, CDSNS, 1998.

[HG94] P. Holmes and R. Ghrist. Knotting within the gluing bifurcaion. In J. M. T. Thompson and S. R. Bishop, editors, *IUTAM Symposium on Nonlinearity and Chaos in Engineering Dynamics*, pages 299–315. John Wiley, Chichester, UK, 1994.

[Hom93] A. J. Homburg. *Some global aspects of homoclinic bifurcations of vector fields*. PhD thesis, Rijksuniversiteit Groningen, 1993.

[HPS70] M. Hirsch, C. Pugh, and M. Shub. *Invariant Manifolds*, volume 583 of *Springer Lecture Notes in Mathematics*. Springer-Verlag, Berlin, Heidelberg, New York, 1970.

[KKO93] M. Kisaka, H. Kokubu, and H. Oka. Bifurcations to n-homoclinic orbits and n-periodic orbits in vector fields. *J. Dynam. Diff. Eqs.*, 5(2):305–357, 1993.

[Kok87] H. Kokubu. On a codimension 2 bifurcation of heteroclinic orbits. *Proc. Japan Acad.*, 63:298–301, 1987.

[Kok88] H. Kokubu. Homoclinic and heteroclinic bifurcations of vector fields. *Japan J. Appl. Math.*, 5:455–501, 1988.

[KRC93] A. Khibnik, D. Roose, and L. Chua. On periodic orbits and homoclinic bifurcations in Chua's circuit with a smooth nonlinearity. *Int. J. Bif. and Chaos*, 3(2):363–384, 1993.

[MP87] E. Meron and I. Procaccia. Gluing bifurcations in critical flows: the route to chaos in parametrically excited surface waves. *Phys. Rev. A*, 35 (9):4008–4011, 1987.

[PTT87] I. Procaccia, S. Thomae, and C. Tresser. First-return maps as a unified renormalization scheme for dynamical systems. *Phys. Rev. A*, 35 (4):1884–1900, 1987.

[RR96] R. Roussarie and C. Rousseau. Almost planar homoclinic loops in $\mathbf{r}^3$. *J. Differential Equations*, 126(1):1–47, 1996.

[San93] B. Sanstede. *Verzweigungstheorie homokliner verdopplungen*. PhD thesis, University of Stuttgart, 1993.

[Thu88] W. Thurston. On the geometry and dynamics of diffeomorphisms of surfaces. *Bull. Am. Math. Soc.*, 19(2):417–431, 1988.